JOURNAL OF SPACECRAFT AND ROCKETS
Vol. 43, No. 4, July–August 2006

Study on Ground Verification for Large Deployable Modular Structures

Akira Meguro*
NTT Corporation, Kanagawa 239-0847, Japan
Hironori Ishikawa†
NTT DoCoMo, Inc., Kanagawa 239-8536, Japan
and
Akio Tsujihata‡
Japan Aerospace Exploration Agency, Ibaragi 305-8505, Japan

A quantitative assessment is provided of the difficulty of ground deployment tests and evaluates the validity of modularized deployment testing for large space structures. An index that well shows the difficulty of ground deployment tests is the ratio of gravity force to deployment force. The relationship between this index and the accuracy of deployment tests is calculated using an analysis model of the large deployable antenna reflectors onboard Engineering Test Satellite VIII (ETS-VIII). The index showed that a deployment structure whose diameter is more than 10 m has insufficient evaluation accuracy; thus the structure should be divided into modules. The index also showed that the single module of the large deployable antenna onboard ETS-VIII is of the appropriate size to evaluate deployment reliability. The influence of module connection on the deployment motion is also examined. The cross correlation between the changes in strain energy profile during deployment in a single module and those in combined modules is calculated to show how many modules should be connected and tested. The resistance force that arose due to the module connection is also calculated using the beam strain energy. It is clarified that ground deployment testing for four combined modules should be conducted in addition to the ground deployment testing for a single module when the deployment force margin is not large enough.

Nomenclature

A = cross-section area
C_M = cross correlation between changes in strain energy profile during deployment in a single module and in combined modules
D_a = deployment force adjusted to agree with experimental results
D_f = true deployment force obtained by microgravity testing
E = Young's modulus
e_E = estimation error of the deployment drive force
f_{eq} = equivalent resistance force
I = second moment of area
i_D = gravity force/deployment force
L = beam length
M = number of combined modules
N = number of data in strain energy profile during deployment used to calculate C_M
P_{beam} = total bending strain energy
p_b = bending strain energy per unit volume
$\bar{p}_i$ = average potential energy in beams during deployment for ith module in isolation
$\bar{p}_i^M$ = average potential energy in beams during deployment for ith module among M combined modules
q = generalized parameter for the system equation of deployment motion
s = hinge displacement
u = translational displacement at edges of a beam
w = mode shape function of a beam
θ = deployment angle
σ_i = standard deviation of potential energy in beams during deployment for ith module in isolation
σ_i^M = standard deviation of potential energy in beams during deployment for ith module among M combined modules
ϕ = rotational displacement at edges of a beam

Presented as Paper 2002-1606 at the AIAA/ASME/ASCE/AHS/ASC 43rd Structures, Structural Dynamics, and Materials Conference, Denver, CO, 22–25 April 2002; received 9 February 2005; revision received 31 October 2005; accepted for publication 4 January 2006. Copyright © 2006 by the American Institute of Aeronautics and Astronautics, Inc. All rights reserved. Copies of this paper may be made for personal or internal use, on condition that the copier pay the $10.00 per-copy fee to the Copyright Clearance Center, Inc., 222 Rosewood Drive, Danvers, MA 01923; include the code 0022-4650/06 $10.00 in correspondence with the CCC.

*Senior Research Engineer and Supervisor, Satellite Communication System Research Group, NTT Network Innovation Laboratory; currently Associate Senior Engineer, Engineering Test Satellite VIII Project, Office of Space Applications, Japan Aerospace Exploration Agency, 2-1-1 Sengen, Tsukuba, Ibaragi 305-8505, Japan.

†Customer Equipment Development Department, 3-5 Hikarinooka, Yokosuka-shi.

‡Senior Engineer, Engineering Test Satellite VIII Project, 2-1-1 Sengen, Tsukuba-city.

I. Introduction

LARGE deployable space structures, such as antenna reflectors, solar paddles, extendable masts, and sun shields, are being developed continuously to support future space activities. They are designed to have sufficient deployment reliability, rigidity, and shape stability against thermal and vibration disturbances. In particular, deployment reliability is the most important factor to be considered to avoid complete mission failure. Therefore, deployment analysis and ground deployment tests should be carefully performed before launch. To perform ground deployment testing for large-scale deployable structures, gravity compensation equipment must be used to avoid excessive gravity loading. Several ground testing arrangements have been created to perform deployment testing.[1,2] Different kinds of suspension systems[3–6] are used for large deployable structures. However, these systems offer only limited gravity compensation, except for some special cases such as function testing for robotic arms.[7] Because many of them cannot support and/or suspend the center of gravity of each moving portion, gravity torque arises around the center of gravity of each moving portion. In addition, it is very difficult to estimate the center of gravity of the entire structure and moving substructures, which changes during deployment motion. The estimation error of the center of gravity significantly

changes the deployment characteristics.[8] In these cases, analysis models are used to evaluate each ground test arrangement. The true characteristics of deployment structures are then extracted from the test results by identifying each system parameter. There are many error sources in this process. For large deployable structures, gravity-induced torque becomes much larger than deployment torque, preventing accurate determination of deployment reliability.

The object of this study is to propose a modularized test method for large deployable structures and to confirm the applicability of the methodology. First, the accuracy of ground deployment testing is considered. A difficulty index, which is defined as the ratio of gravity-induced deployment force and deployment force, is proposed for ground deployment testing. The index shows the limit of each ground deployment test arrangement in terms of a structural metric. Second, the relationship between the index value and the accuracy of the deployment characteristic, evaluated using test results, is quantitatively estimated. Next, the cross correlation between the changes in strain energy profile during deployment in a single module and those in combined modules is calculated to show how many modules should be connected and tested. Finally, the resistance force due to the module connection is also calculated using the beam strain energy to show that the cross-correlation value directly indicates the variance of the deployment force margin.

II. Conventional Ground Test Methods

Conventional ground test methods for antenna reflectors can be divided into the following two examples according to the size of antenna reflectors.

A. Relatively Small Deployable Antenna Reflector

Only a few deployment structures can be deployed in one plane, such as relatively small rigid antenna reflectors, solar array panels, booms, and masts. For these relatively simple deployment structures, the system identification method[9] can be employed. The Engineering Test Satellite VI (ETS-VI) was launched in 1994 by the Japanese H-II launch vehicle. It had two large deployable main reflectors and two deployable subreflectors (Fig. 1). The largest reflector was 3.5 m in aperture diameter. All system parameters, including the air drag and gravity compensation errors, were considered in the system equation of deployment motion

$$I\ddot{\theta} = q_1 + q_2\theta + q_3\dot{\theta}^2 + q_4\dot{\theta} + q_5 \sin(q_6\theta + q_7) \qquad (1)$$

where q_1 and q_2 are the driving force (including friction force and resistance forces) and spring constant, respectively; $q_3\dot{\theta}^2$ and $q_4\dot{\theta}$ are aerodynamic effects, and $q_5 \sin(q_6\theta + q_7)$ represents the effects of the gravity cancellation equipment. Only two parameters, q_1 and q_2, represent the deployment characteristics of the reflector being evaluated. They were retrieved from the results of ground deployment tests conducted on different test configurations. Through launch survival testing and thermal/vacuum testing, it was possible to confirm that the antenna reflectors had a sufficient deployment force margin. In-orbit deployment time of the reflectors was accurately predicted, as shown in Table 1.[10] In this table, σ denotes the standard deviation of driving torque measured by ground deployment testing. For the deployment mechanism used for ETS-VI, average torque was around 2 N · m and the 1σ was around 0.2 N · m.

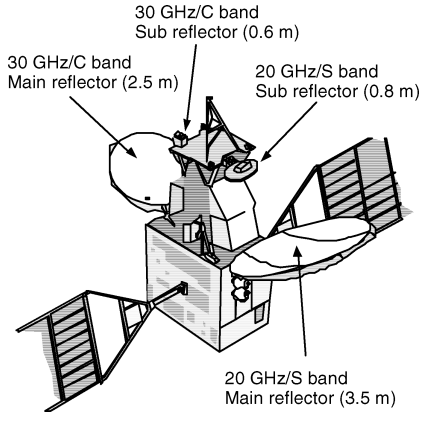

Fig. 1 Deployable antenna on board ETS-VI.

Table 1 In-orbit deployment time of the reflectors

Event	Measured deployment time, s	Predicted deployment time, s				
		-2σ	-1σ	mean	$+1\sigma$	$+2\sigma$
$-Y$ wing part	2.0[a]	2.1	2.0	1.9	1.9	1.8
$+Y$ wing part	2.0[a]	2.2	2.1	2.0	1.9	1.9
3.5-m main ref	20.0	26.5	23.5	21.4	19.7	18.4
2.5-m main ref	8.9	11.2	10.3	9.7	9.1	8.6

[a] $+Y$ wing and $-Y$ wing are not distinguished.

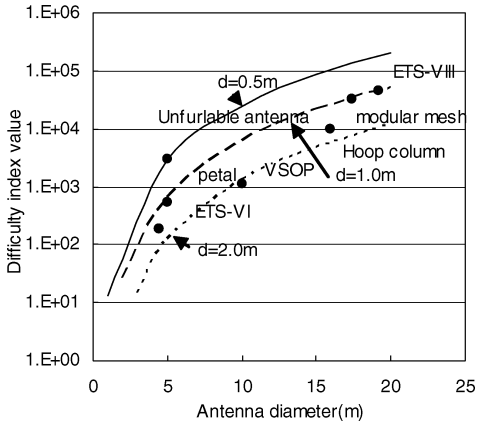

Fig. 2 Difficulty index value.

B. Large Scale Deployable Antenna Reflectors

The system identification method cannot be used for complicated deployment structures such as deployable truss/frame structures, because the system equation of deployment motion is too complicated to describe explicitly. A common solution is to use the finite element method. The model is correlated to the test results to predict in-orbit deployment motion. However, this method does not have sufficient accuracy even for small deployment structures. A scaled model of the basic module of the large deployable reflector (LDR) of the Engineering Test Satellite VIII (ETS-VIII) was tested by the Japan Aerospace Exploration Agency (JAXA) in a microgravity environment created within a jet airplane, an A300. The estimation error, which was found to be about 10%, was due to the approximations used to model nonstructural mass elements (such as mesh and cables). For the full-scale reflector, whose size is 19×17 m, it becomes virtually impossible to evaluate its actual characteristics. Very large, complicated gravity compensation arrangements are needed to perform ground deployment tests. In these cases, the engineers are actually evaluating the characteristics of the ground test system, instead of evaluating those of the reflector. Therefore, the accuracy of ground deployment testing must be examined. If the estimation error is several tens of percent of the designed deployment force, design engineers must add more force margin to the nominal design values. If the error is several hundreds of percent of designed deployment force, design engineers must divide the structure into modules of appropriate size or they cannot trust the test results.

III. Difficulty Index and Evaluation Accuracy

A. Difficulty Index Value

When the deployment test is considered, the quantity i_D, the ratio of the gravity-induced force to the deployment force, is an index of the difficulty of the ground deployment test.

$$i_D = \frac{\text{gravity force}}{\text{deployment force}} \qquad (2)$$

As shown in Fig. 2, Mitsugi defined the index of difficulty of deployment test as a function of the size of the deployable structure

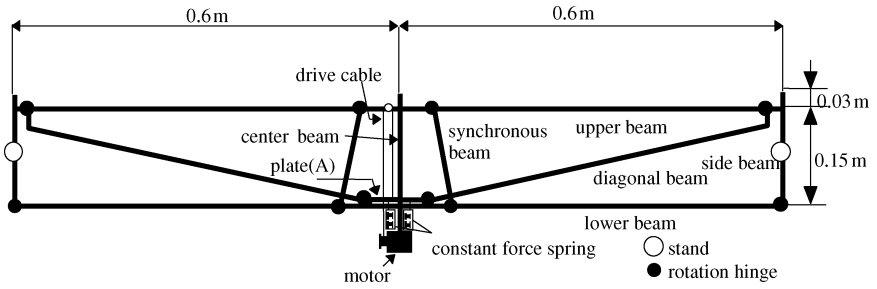

Fig. 3 Simple planar truss.

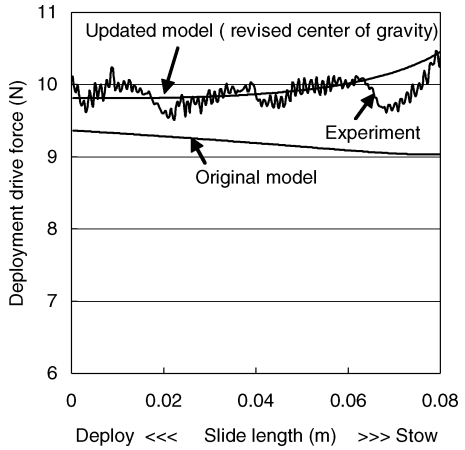

Fig. 4 Result of the updated analysis model.

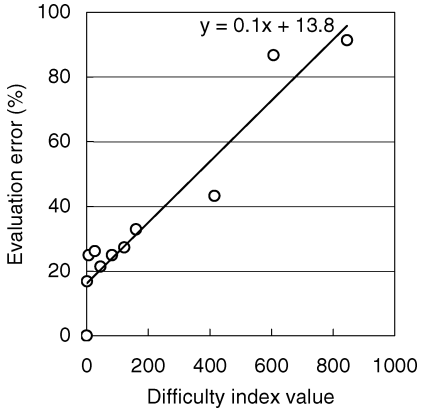

Fig. 5 Relationship obtained between the difficulty index value and the evaluation accuracy.

as the equation[11]

$$i_D = 2D^2(D-d)/0.3d^2 \tag{3}$$

where D is the antenna diameter and d is the stowed diameter. The index showed that test engineers could not accurately measure the deployment drive force of deployable structures that were more than 10 m in diameter. The basis of this metric is that conventional measurement systems have dynamic ranges between 1000 and 10,000. However, the quantitative relationship between deployable structure size and evaluation accuracy remained unclear.

B. Simple Planar Truss Experiment

A simple planar truss experiment was performed to evaluate the relationship between the difficulty index value and the accuracy of deployment testing on the ground.[12] The difficulty index value was obtained by calculating an analysis model under $1g$ and $0g$ conditions. Figure 3 shows the simple planar truss, which was designed and fabricated based on the deployable truss support structure of the modular mesh antenna developed by Nippon Telegraph and Telephone Corporation (NTT).[13,14] To change the difficulty index value, additional weights were installed on each side beam, and the constant-force spring was changed. Two kinds of deployment testing were performed. One was performed in a microgravity environment obtained by parabolic flights of a jet airplane, MU300, and the other was performed on the ground. Assuming that the deployment characteristics measured under microgravity represent the true deployment characteristics of the planner truss, the accuracy of ground deployment testing was evaluated.

Figure 4 shows the experimental results obtained by ground testing. The analysis results are also plotted to show the prediction accuracy. There is approximately 10% difference between the experimental and analysis results, even though the "true" deployment force was used in the analysis model. The reasons for the difference are thought to be modeling inaccuracies of the suspension system and the center of gravity of the planner truss. In this ground deployment test, the suspending position and the tension of suspension wires were measured within 1% and 0.1% error, respectively.[15] Total weight was measured within 0.1% error, and inertial moment was negligibly small in this deployment testing. Finally, the center of gravity of the planar truss was measured. The weight at each suspension position was directly measured. The difference in weight of the analysis model was approximately 0.02 kg (9%) even though the weights of the analysis model matched those of each beam. The results of the updated analysis model are also shown in Fig. 4. The analysis model shows good agreement with the experimental results. This agreement proves that accuracy of the analysis prediction is mainly determined by the accuracy of estimating the center of gravity of the planar truss. Unfortunately, measuring the center of gravity of large deployable structures is extremely difficult, and usually such measurements are not conducted. Accordingly, the mass properties of the deployable structure must be assumed to contain some inaccuracy. This inaccuracy means that there is no basis for correlating results from the analysis model to adjustments in mass properties. The analysis model must be correlated by adjusting the deployment force so that the estimate provides a reasonable safety margin. Given this argument, it should be expected that a 10% difference between the experimental and the analysis results will be inevitable due to the inaccuracy of the deployment force in Fig. 4. Consequently, the accuracy of deployment testing was defined as

$$(D_a - D_f)/D_f \times 100\,(\%) \tag{4}$$

where D_a denotes the deployment force adjusted to achieve agreement with the experimental results and D_f denotes the true deployment force obtained by microgravity testing. The relationship obtained between the difficulty index value and the evaluation accuracy is shown in Fig. 5. The estimation error of the deployment drive force is approximately 14% for the difficulty index value of 0. Assuming a linear relation between index value and estimation error e_E, the following empirical equation can be obtained:

$$e_E = 0.1 i_d + 14\,(\%) \tag{5}$$

where i_d represents the difficulty index value. The estimation error of the deployment drive force exceeds 100% when the difficulty index value = 900. In general, design engineers can redesign a mechanism giving additional torque margin when the estimation error is around

20%; however, they cannot accept an estimation error of 100%. Therefore, the size of test articles should be reduced to keep the difficulty index value around 100. Consequently, the authors suggest module-based deployment testing as one of the best solutions to evaluate deployment characteristics of large deployable space structure on ground.

IV. Modular Structure for Large Deployable Antenna Reflector On Board ETS-VIII

A. Module Design and Analysis Model

The modular configuration was employed in creating the large deployable reflector (LDR) onboard ETS-VIII, which is being developed by JAXA and will be launched in 2006. Figure 6 shows the in-orbit system configuration of ETS-VIII. Two LDRs are to be used for mobile communication and broadcasting experiments. As shown in Fig. 7, each LDR consists of 14 basic modules, each of which is about 5 m in diameter. Each basic module consists of a cable-mesh reflector and a deployable support structure. As shown in Fig. 8, the basic modules consist of cables, mesh, and the deployable support structure that gives tension to the cables. A system of cables form a mesh into a parabolic shape. The deployable support structure is designed to have a spherical shape, which is best fitted to a given parabolic surface. Therefore, standoffs are used to connect the cable-mesh structure to the deployable support structure by filling in the difference between a parabolic surface and a spherical surface.[16,17] Figure 9 explains the design rules for module arrangement. There are only three simple rules to determine each nodal position on an upper surface of a deployable support structure. Rule A is that every rib member has the same length but not all ribs need necessarily have the same relative angle. Rule B is that every node is located on a predetermined spherical surface, and the relative angle of a pair of specific ribs can be given in the x–y plane. Rule C is that every node is located on a predetermined spherical surface, and a node is located equidistant from two predetermined nodes, where the distance equals rib length. For example, node 0 can be defined as the origin of the x–y coordinate at first. Next, nodes 1 and 2 can be determined by rule B, and node 3 can be determined by rule C. The other nodes are determined in the same manner.

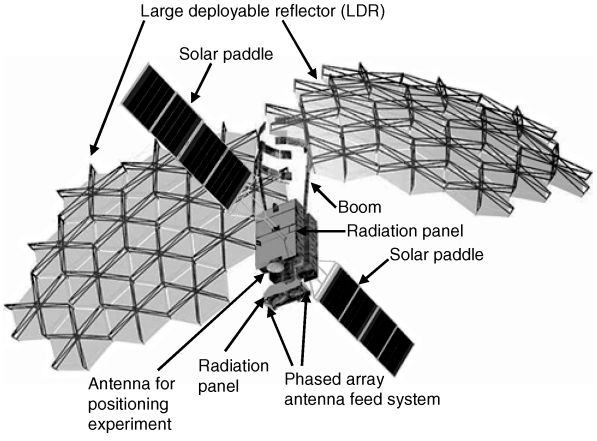

Fig. 6 In-orbit configuration of ETS-VIII.

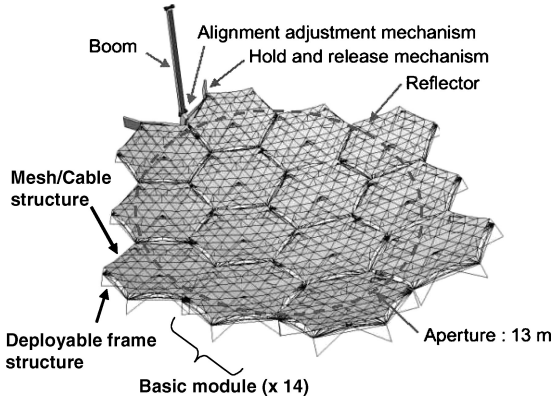

Fig. 7 Large deployable antenna reflector.

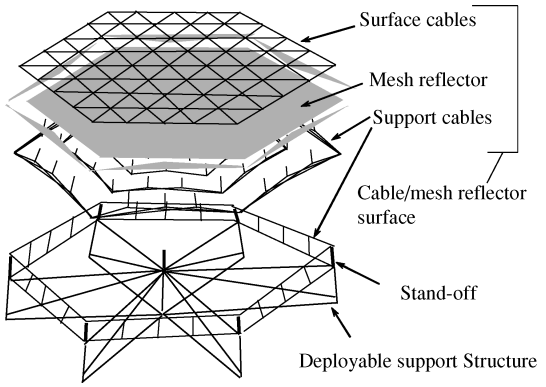

Fig. 8 Detail of basic module.

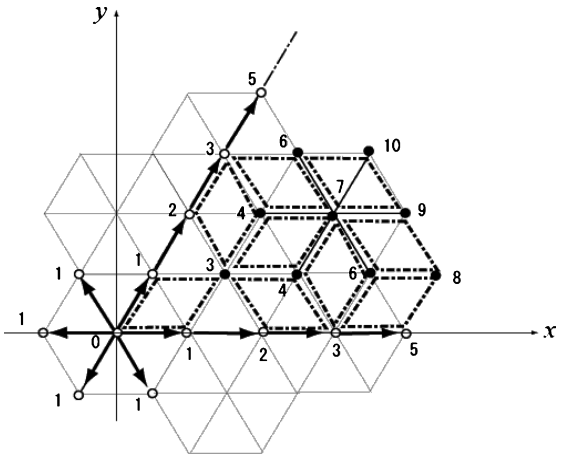

Fig. 9 Design role for module arrangement.

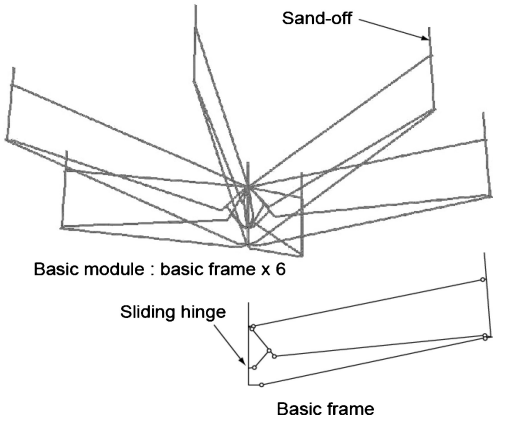

Fig. 10 Analysis models of a basic frame and a basic module.

An analysis model was constructed by using the in-house analysis tool SPADE (simple coordinate partitioning algorithm-based dynamics of finite elements).[18,19] SPADE can analyze the deployment behavior of elastic structures that consist of beams, rods, plates, cables, and membranes. Figure 10 shows analysis models of a basic frame and a basic module, respectively. The model consists of elastic beams connected by weld, revolute, and cylindrical (sliding) hinges. The basic frame structure is stowed by moving the slide hinge upward. The basic module consists of six basic frames arranged spokewise around the central axis.

Table 2 Deployment test steps for the EM of LDR

Test step	Number of modules	Test equipment (gravity canceller)	Test results
1	1	Fixed suspension system using a simple test rig	Fig. 12
2	3	Moving suspension system (passive tracking)	Fig. 13
3	7	Moving suspension system (active tracking)	Fig. 14

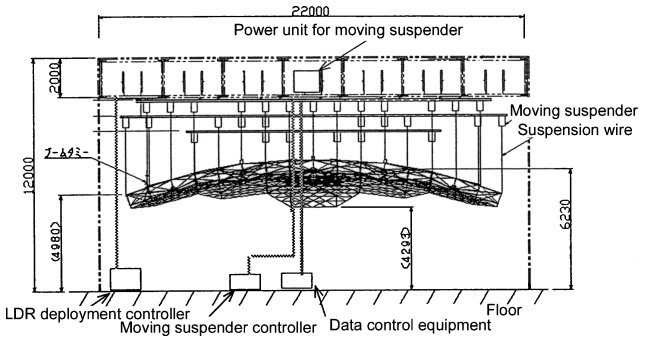

Fig. 11 Moving suspension system for LDR.

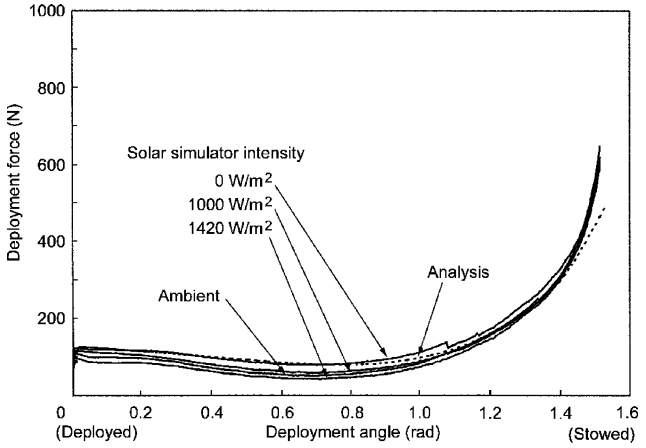

Fig. 12 Driving force obtained by ground deployment testing for single module.

B. Accuracy of Deployment Testing

A full-scale engineering model (EM) for LDR has been tested step by step. Table 2 shows deployment test steps for the EM of LDR. In the first step, deployment tests were performed on a single module by means of a fixed suspension system using a simple test rig. Figure 11 shows resulting deployment force profiles for the single module. In the second, third, and fourth steps, 3, 7, and 14 combined modules were tested, respectively, using the moving suspension system shown in Fig. 12. Figures 13 and 14 show resulting deployment force profiles for three and seven modules, respectively. The resulting deployment force profile changed remarkably after the third step. The difficulty index value in each test step was calculated by analyzing the deployment force profile in the gravity environment without any gravity compensation. Figure 15 shows the difficulty index value at each test step. The evaluation accuracy is calculated using Eq. (5), assuming a linear relationship between the difficulty index and the evaluation accuracy. The evaluation accuracy also indicated on the right side of the vertical line. This figure clarifies that the evaluation accuracy would be insufficient if ground deployment testing is performed on more than three combined modules. For example, the maximum difference between the test results and the analysis results shown in Fig. 14 is around 50%. The evaluation accuracy obtained by ground deployment test double the accuracy predicted by an empirical equation, because Eq. (5) was obtained by

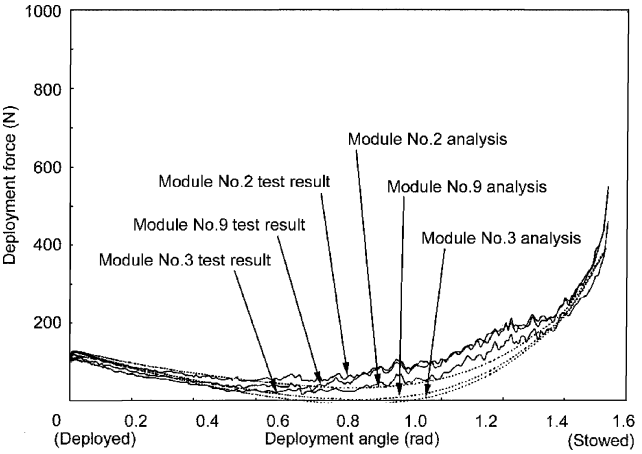

Fig. 13 Deployment force profile of three-module assembly.

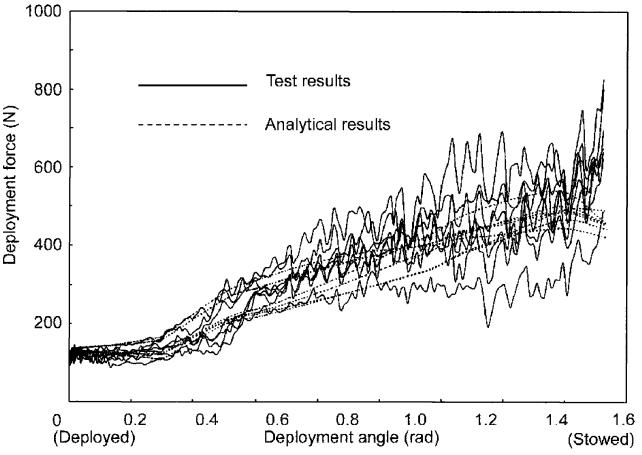

Fig. 14 Deployment force profile of seven-module assembly.

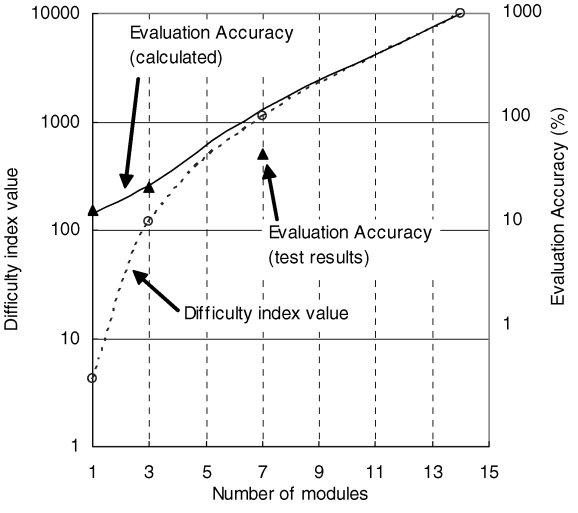

Fig. 15 Evaluation accuracy of LDR on board ETS-VIII.

an extremely simple deployable structure. Equation (5) should be improved by using other measured data; however, it is obvious that the evaluation error of the seven combined modules is considerably large. It is recognized, of course, that ground deployment testing is still necessary to find errors in workmanship and/or interference with nonstructural elements. However, it should be noted that only a few deployment characteristics of large structures can be evaluated by ground deployment testing. It is also recognized that the single module of the LDR was the optimal size for evaluating deployment

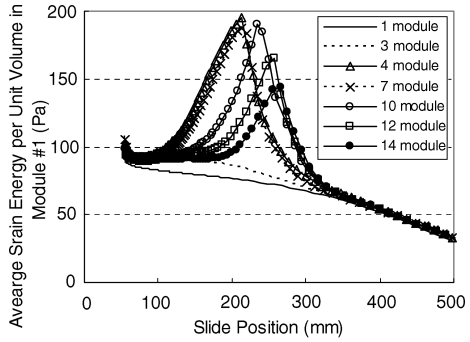

Fig. 16 Influence of module connection on strain during deployment.

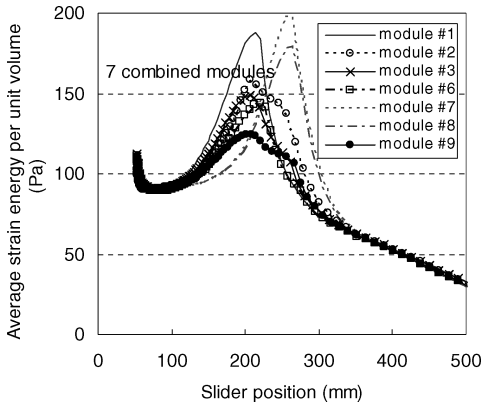

Fig. 17 Average strain energy in seven combined modules during deployment.

reliability; we note that if ground deployment testing examined just seven or more combined modules, the resulting evaluation accuracy would be insufficient.

C. Cross Correlation Between an Isolated Module and a Combined Module

Because of its spherical nature, the designed structure must be deformed during deployment. In contrast, the basic module is not deformed because the module consists of frame structures arranged around a center axis. Therefore, the influence of module connection appeared in the changes in strain energy in structural members during deployment. Figure 16 shows the relationship between the number of connected modules and the beam strain energy during deployment. In Fig. 16, the index of strain energy is represented by the average strain energy, which is defined as the average of strain energy for each unit volume in each structural member, calculated at each deployment position by SPADE. The average strain energy in module 1 changes when the number of connected modules increases. The maximum peak appears when four modules are combined; the peak decreases as the number of modules increases thereafter. Furthermore, Fig. 17 shows the variation of beam strain energy only in module 1; however, the strain energy varied among connected modules. The difference in strain energy between modules in 7 and 14 connected modules is shown in Figs. 17 and 18, respectively. By comparing Figs. 17 and 18, it is noted that the dispersion of the strain energy also becomes small when a larger number of modules are connected. Next, the relationship between the module design and the beam strain energy was examined. Figure 19 shows module numbering and variation in relative angle between each rib. The relative angle between ribs varies with location due to the modular design as described in Sec. IV.D. The value was calculated as the standard deviation of rib angles in each module. Figure 19 also shows the distribution of average strain energy per unit volume. Any relationship between variation in rib angle and strain energy cannot be found. Instead, it is noted that enclosed modules show higher strain energy than circumferential modules.

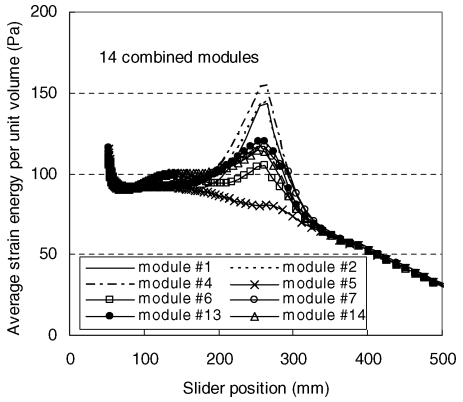

Fig. 18 Average strain energy in seven combined modules during deployment.

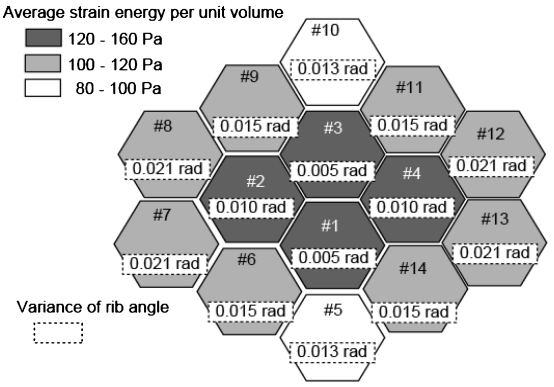

Fig. 19 Module numbering and distribution of average strain energy per unit volume.

To establish a design methodology for the module structure, the quantitative relationship between the deployment characteristics of a single module and those of combined modules was examined. A cross correlation between the changes in strain energy profile during deployment in a single module and those in combined modules was derived from analysis results as follows:

$$C_M = \frac{1}{\sigma_i^M \sigma_i} \frac{1}{N} \sum_{x=1}^{N} \left(p_i^M[x] - \bar{p}_i^M\right)(p_i[x] - \bar{p}_i) \tag{6}$$

$$\bar{p}_i^M = \frac{1}{N} \sum_{x=1}^{N} p_i^M[x] \tag{7}$$

$$\sigma_i^M = \sqrt{\frac{1}{N} \sum_{x=1}^{N} \left(p_i^M[x] - \bar{p}_i^M\right)^2} \tag{8}$$

$$\bar{p}_i = \frac{1}{N} \sum_{x=1}^{N} p_i[x] \tag{9}$$

$$\sigma_i = \sqrt{\frac{1}{N} \sum_{x=1}^{N} \left(p_i[x] - \bar{p}_i\right)^2} \tag{10}$$

where $\bar{p}_i^M$, σ_i^M are average and standard deviation of potential energy in beams during deployment for the ith module among M combined modules, respectively, and $\bar{p}_i$, σ_i are those for the ith module in isolation.

Figure 20 shows the relationship between the number of combined modules and the cross-correlation coefficient between a single module and a combined module. The cross-correlation coefficient

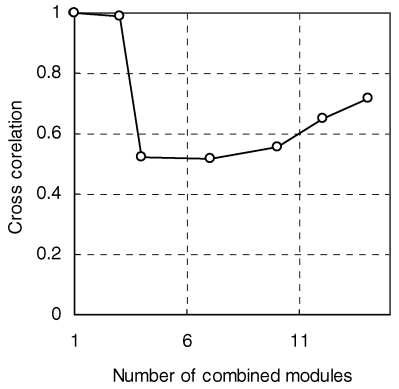

Fig. 20 Cross-correlation coefficient between an isolated module and a combined module.

suddenly decreases to around 0.5 when four modules are combined, and gradually increases thereafter as the number of combined modules increases. The relationship shown in Fig. 20 means that the combined modules, which consist of four modules, must be tested on the ground, in addition to testing for a single module. In other words, ground deployment testing for the combined modules which consist of more than five modules is not needed from a viewpoint of deployment force margin.

D. Influence of Module Connection on Deployment Characteristics

As described in the Sec. IV.C, the cross correlation between the changes of strain energy in a single module and in combined modules would rapidly decrease to 0.5 when four modules were combined. From a viewpoint of deployable reliability, this decrement means that the necessary force margin is double that designed for a single module. In this section, the relationship between the beam strain energy and the resistance force against deployment motion is examined to estimate the influence of module connection more clearly. To understand the influence of module connection number on deployment characteristics, a resistance force against deployment motion was calculated by using strain energy. When internal force arises due to module connection in a deployable structure during deployment, two major resistance factors affect the deployable characteristics. One is friction torque and/or force in each hinge portion. The other is the dissipation of deployment energy due to structural deformation. First, using a simple analysis model, the resistance force reflected in the sliding hinges due to friction was estimated quantitatively. The mode shape function expressed as Hermite's polynomial is

$$w(x) = [1 - 3(x^2/L^2) + 2(x^3/L^3)]u_1 + [3(x^2/L^2) - 2(x^3/L^3)]u_2 + [-x + 2(x^2/L) - (x^3/L^2)]\phi_1 + (x^2/L - x^3/L^2)\phi_2 \quad (11)$$

where L is beam length and u, ϕ are translational and rotational displacements, respectively. Assuming the boundary condition on both edges is simple support and that the beam has uniform cross section, the following relationship can be derived:

$$\frac{\partial^2 w}{\partial x^2} = \frac{2}{L}\phi \quad (12)$$

This relationship means that a uniform moment M arises along the beam when Young's ratio E and the second moment of area I in the y–z plane of area A are uniform along the beam. The bending strain energy per unit volume, p_b, can be formulated as

$$\phi = \frac{1}{2A}\iint Ez^2\left(\frac{\partial^2 w}{\partial x^2}\right)^2 \mathrm{d}y\,\mathrm{d}z = \frac{1}{2A}EI\left(\frac{\partial^2 w}{\partial x^2}\right)^2 \frac{M^2}{2EAI} \quad (13)$$

Consequently, bending moment M can be expressed using p_b as $M = \sqrt{(2EAIp_b)}$. As shown in Figs. 16 and 17, the maximum value of average strain energy per unit volume is around 200 Pa. Here, it must be noted that the strain energy in a single module arises only from springs that produce deployment force. Therefore, the maximum value of strain energy due to module connection is around 100 Pa, excluding strain energy from springs. Using the material and cross-sectional properties of the members in the analysis model ($E = 2 \times 10^{11}$ Pa, $A = 3 \times 10^{-7}$ m^2, $I = 3 \times 10^{-9}$ m^4), the moment is estimated to be around 0.15 N · m. Assuming the coefficient of friction to be about 0.1, the friction torque around the hinge axis is estimated to be 0.015 N · m. Figure 21 shows the influence of the friction torque on the driving force of the slider of a single module. Comparing this result to the minimum driving force of around 50 N obtained by ground deployment testing for the single module shown in Fig. 11, it is obvious that the driving force has sufficient force margin against the resistance forces.

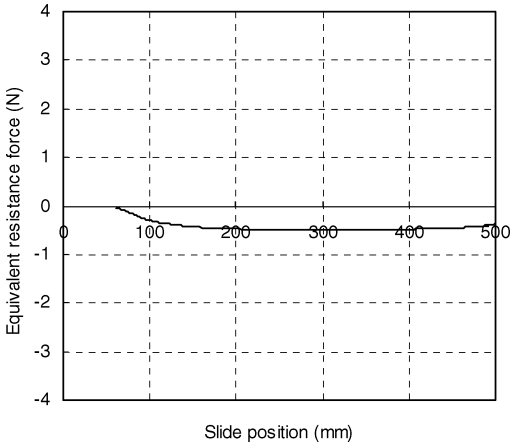

Fig. 21 Friction force in sliding hinges calculated using the beam strain energy.

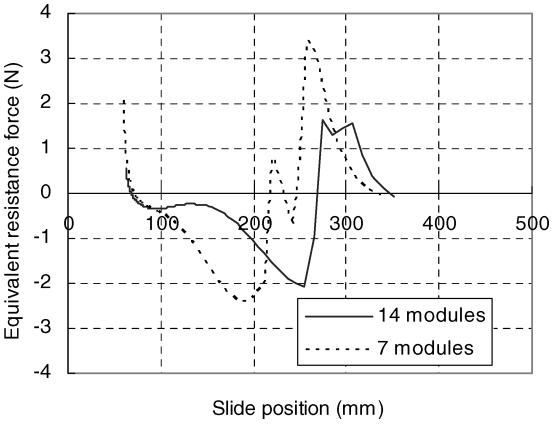

Fig. 22 Resistance force in sliding hinges due to the dispersion of the beam strain energy.

On the other hand, the change in strain energy with displacement of the sliding hinge during deployment can represent deployment force or resistance force. The changes in strain energy are generated by the following factors: 1) structural deformation due to geometrical incompatibility during deployment; 2) elongation of cable elements in the reflector structure; 3) springing back of drive-spring elements. Among these factors, 1 and 2 show positive changes, and 3 shows negative change. In this analysis, 2 and 3 are eliminated from the analysis model to clarify the influence of module connection on the deployment characteristic. The equivalent resistance force f_{eq} can be obtained as

$$f_{\mathrm{eq}} = \Delta P_{\mathrm{beam}}/M\Delta s \quad (14)$$

where ΔP_{beam} is the change in total beam strain energy at each calculation step, Δs is the change in slider position at each calculation step, and M is the number of modules. Figure 22 shows equivalent resistance force in the sliding hinges as a function of slide position.

The peak resistance force, around 2.5 N, is larger than the friction torque, but it is small enough compared to the driving force of ETS-VIII as shown in Fig. 12. The ratio of the maximum resistance force in 7 combined modules to that in 14 combined modules is $3.4/2.1 = 1.6$, whereas the ratio of the cross-correlation value of 7 modules and that of 14 modules is $(1/0.5)/(1/0.72) = 1.4$. These two ratios almost agree with each other. This agreement shows that the cross correlation between the strain energy in a single module and that in combined modules well shows the influence of the module connection, and the minimum deployment force margin appears in four combined modules. Consequently, it can be concluded that if the deployment force margin is not large enough, the ground deployment testing for four combined modules should be conducted in addition to the ground deployment testing for a single module.

V. Conclusions

The difficulty index value of the modularized large deployable reflectors for ETS-VIII and the influence of module connection on the deployment motion were examined in this paper using analysis models. The following conclusions are obtained:

1) The difficulty index of a deployment structure, whose diameter is more than 10 m, shows that the evaluation error would be excessive, several tens of percent of the designed deployment force. Therefore, module-based deployment testing is one of the best solutions in evaluating deployment characteristics on the ground.

2) The difficulty index of the modularized LDR for ETS-VIII was calculated. The single module of the LDR, which was about 5 m in diameter, was designed to be of appropriate size to allow accurate ground evaluation testing of the deployment reliability.

3) To show the quantitative relationship between the deployment characteristics of a single module and those of combined module, the cross correlation between the changes in strain-energy profile during deployment in a single module and those in combined modules was derived from analysis results. The calculated values show that ground deployment testing for the combined modules which consists of more than five modules is not needed from a viewpoint of deployment force margin.

4) The resistance force against the deployment motion mainly arises by the dissipation of deployment energy due to structural deformation. The ratio of the maximum resistance force in 7 combined modules to that in 14 combined modules is 1.6, whereas the ratio of the cross-correlation value of 7 modules and that of 14 modules is 1.4. This agreement shows that the cross correlation between the strain energy in a single module and that in combined modules directly shows the variance of deployment force margin, and the minimum deployment force margin appears in four combined modules.

5) As for the LDR on board ETS-VIII, each single module has a sufficient force margin; however, if the deployment force margin is not large enough, the ground deployment testing for four combined modules should be conducted in addition to the ground deployment testing for a single module.

Acknowledgments

The authors thank Masanori Honma, Project Manager of Engineering Test Satellite VIII, JAXA, for his support and advice to our study. The authors thank members of the LDR design team, NEC Toshiba Space Systems, for their suggestion and fruitful discussion. The authors also thank Masanori Umehira and Masazumi Ueba, NTT Network Innovation Laboratories, NTT Corp., for their support.

References

[1]Hanks, B. R., and Pison, L. D., "Large Space Structure Raise Testing Challenges," *Astronauts and Aeronautics*, Oct. 1983, pp. 34–53.

[2]Hanks, B. R., "Control of Flexible Structure (COFS) Flight Experiment—Background and Description," *Proceedings Large Space Antenna Systems Technology,* NASA CP-2368-PT-2, Dec. 1984, pp. 893–908.

[3]Brazzini, G., Broustet, Y., Garnier, C., and Picard, P., "Kinematic Analysis of Large Deployable Truss Antenna," *Proceedings of the 36th International Astronautical Congress*, IAF-85-74, International Astronautical Federation, Paris, 1985.

[4]Stella, D., Morgan, F., and Nielsen, G., "Contraves' Antenna Tip Hinge Mechanism for Selenia Spazio's 20/30 GHz Antenna," *Proceedings of the 2nd ESA Workshop Mechanical Technology for Antenna*, ESA SP-261, Aug. 1986, pp. 185–194.

[5]Lemak, M. E., and Banerjee, A. K., "Comparison of Simulation with Test of Deployment of a Wrapped-Rib Antenna," *Proceedings of AIAA Guidance, Navigation, and Control Conference*, AIAA, Washington, DC, 1994, pp. 327–337.

[6]Dotson, R. D., "Spacecraft Deployable Structure Testing," *Proceedings of the AGARD Flight Vehicle Integration Panel Symposium on "Space System Design and Development Testing*," CP-561, 1994, pp. 6-1–6-12.

[7]Brown, H. B., Jr., and Dolan, J. M., "A Novel Gravity Compensation System for Space Robots," *Proceedings of the Robotics for Challenging Environments*, American Society of Mechanical Engineers, New York, 1994, pp. 250–258.

[8]Meguro, A., Ishikawa, H., Tsujihata, A., Miyasaka, A., and Nakamura, K., "Analysis and Test Methods for Large Deployable Space Structures," *Proceedings of the 42nd AIAA/ASME/ASCE/AHS/ASC Structures, Structural Dynamics, and Materials Conference*, Vol. 42, No. 3, AIAA, Reston, VA, 2001, pp. 2212–2221.

[9]Meguro, A., and Mitsugi, J., "Ground Verification of Deployment Dynamics of Large Deployable Space Structures," *Journal of Spacecraft and Rockets*, Vol. 29, No. 6, 1992, pp. 835–841.

[10]Meguro, A, "In-Orbit Deployment Performance of Large Satellite Antennas," *Journal of Spacecraft and Rockets*, Vol. 33, No. 2, 1996, pp. 222–227.

[11]Mitsugi, J., and Yasaka, T., "Deployable Modular Mesh Antenna—Concept and Feasibility," *Proceedings of the 17th International Symposium on Space Technology and Science*, Vol. 1, ISTS Secretariat, Tokyo, 1990, pp. 599–604.

[12]Meguro, A., Ishikawa H., and Tsujihata, A., "A Study on the Accuracy of Deployment Testing for Large Deployable Structures," *Proceedings of the 43rd AIAA/ASME/ASCE/AHS/ASC Structures, Structural Dynamics, and Materials Conference*, Vol. 43, No. 5, AIAA, Reston, VA, 2002, pp. 3107–3116.

[13]Meguro, A., Mitsugi, J., Miyasaka, A., and Watanabe, M., "Development of 15m Class Modular Mesh Deployable Antenna," *Proceedings of the 48th International Astronautical Congress*, IAF-97-I.1.09, International Astronautical Federation, Paris, 1997.

[14]Watanabe, M., Meguro, A., Mitsugi, J., and Tsunoda, H., "Module Composition and Deployment Method on Deployable Modular-Mesh Antenna Structures," *Acta Astronautica*, Vol. 39, No. 7, 1996, pp. 497–505.

[15]Ishikawa, H., and Meguro, A., "High Accuracy Evaluation Method of Deployment Characteristics for Large Deployable Structures," *Proceedings of the 9th European Space Mechanisms and Tribology Symposium*, ESA Publication Division, Noordwijk, The Netherlands, 2001, pp. 137–144.

[16]Meguro, A., Tsujihata, A., and Hamamoto, N., "The 13 m Aperture Space Antenna Reflector for Engineering Test Satellite VIII," *Proceedings of the IEEE AP-S*, AP-64, Vol. 1999, No. 3, Inst. of Electrical and Electronics Engineers, New York, 1999, pp. 1520–1523.

[17]Meguro, A., Tsujihata, A., Hamamoto, N., and Homma, M., "Technology Status of the 13 m Aperture Deployment Antenna Reflectors for Engineering Test Satellite VIII," *Acta Astronautica*, Vol. 47, Nos. 2–9, 2000, pp. 147–152.

[18]Mitsugi, J., "Direct Coordinate Partitioning for Multibody Dynamics Based on Finite Element Method," *Proceedings of the 36th AIAA/ASME/ASCE/AHS/ASC Structures, Structural Dynamics, and Materials Conference*, AIAA, Washington, DC, 1995, pp. 2481–2487.

[19]Misugi, J., and Senbokuya, Y., "Dynamic Analysis of Cable-Driven Flexible Multibody Systems and Its Experimental Verification," *Proceedings of the 37th AIAA/ASME/ASCE/AHS/ASC Structures, Structural Dynamics, and Materials Conference*, AIAA, Reston, VA, 1996, pp. 1530–1535.

G. Agnes
Associate Editor